Turk. J. Fish.& Aquat. Sci. 23(2), TRJFAS21398
https://doi.org/10.4194/TRJFAS21398

RESEARCH PAPER

Turkish Journal of FISHERIES and AQUATIC SCIENCES

Biogenic Synthesis of Iron Oxide Nanoparticle Using *Padina Pavonica* Extract: Application for Photocatalytic Degradation of Congo Red Dye, Neurotoxicity and Antioxidant Activity

Fatma Caf[1,*]

[1]University of Bingöl, Vocational School of Food, Agriculture and Livestock, 12000, Turkiye

How to cite

Caf, F. (2023). Biogenic Synthesis of Iron Oxide Nanoparticle Using *Padina Pavonica* Extract: Application for Photocatalytic Degradation of Congo Red Dye, Neurotoxicity and Antioxidant Activity *Turkish Journal of Fisheries and Aquatic Sciences*, *23(2)*, *TRJFAS21398.*
https://doi.org/10.4194/TRJFAS21398

Article History
Received 07 February 2022
Accepted 07 September 2022
First Online 22 September 2022

Corresponding Author
Tel.: +905306576390
E-mail: f.baydas23@hotmail.com

Keywords
Green synthesis
P. pavonica
Dye degradation
SH-SY5Y
Antioxidant activity

Abstract

The current study focused on green synthesis of iron nanoparticles by *Padina pavonica* (Pa@FeNPs), removal activity of dye CR (Congo Red) and investigating antioxidant and neurotoxicity activities. The morphological and physical properties of Pa@FeNPs were characterized by FT-IR (Fourier Transform Infrared Spectroscopy), XRD (X-Ray Diffractometer), SEM (Scanning Electron Microscopy), EDX (X-Ray Spectroscopy), TEM (Transmission Electron Microscopy) and Zeta potential analyses. XRD and zeta potential analyses revealed a potential of-8.53 mV and formation of cubic crystals with an average dimension of 10.53-20.55 nm. The optimum conditions of pH, temperature, initial dye concentration and adsorbent amount for CR removal were found to be 4, 40°C, 20 ppm and 20 mg respectively. The CR removal percentage using Pa@FeNPs reached a very high efficiency of 95%. Langmuir Isotherm model (R^2=0.99, 25°C) was best fitted to our data for evaluating dye adsorption behaviors of the Pa@FeNPs. Metal chelating activity in the aqueous extract of *P. pavonica* and Pa@FeNPs was found to be 74.71±2.16% and 64.95±0.42%, respectively. Inhibitory concentration 50 (IC_{50}) values for *P. pavonica* aqueous extract and Pa@FeNPs were found to be 0.128 µg/mL and 400 µg/mL, respectively in the SH-SY5Y (Human neuroblastoma).

Introduction

The green synthesis method utilizing chemical processes inherent to living organisms enables to create complex products derived from simple substances. The green synthesis method can produce biocompatible nanomaterials with low ecotoxicity since harmful waste generation is minimized (Bhattacharjee et al., 2021). The increasing interest in green chemistry and other biological processes have led scientists to synthesize environmentally friendly nanoparticles that are simple, affordable, compatible with biomedical and pharmacological applications, and that has many advantages including being suitable for commercial production in a wide range of applications (Flippo et al., 2010). Some studies related to the green synthesis method employing metal nanoparticles with different biogenic substances have been reported in a wide variety of scientific fields (Neshastehriz et al., 2020; Amini et al., 2021; Rezaeian et al., 2021; Mohammadi et al., 2021).

One of the biogenic materials that can be used for this purpose is marine alga. Algae can exhibit antimicrobial, antioxidant, anti-inflammatory, anti-aging, anti-viral, antifungal, antibacterial, and anti-cancer activities. These activities are attributed to presence of bioactive functional groups such as amine, sulfate, carboxyl, and hydroxyl groups (Azizi et. al., 2014). Biological materials contain various secondary metabolite compounds that act as both encapsulating and reducing agents to form nanoparticles (Sathiyavimal et al., 2018). Besides the reduction, secondary metabolites surround the nanoparticles, providing stability and unique morphological properties (Varadavenkatesan et al., 2019).

Using algae to prepare nanoparticles is more advantageous than other biological sources such as bacteria and fungi as they eliminate the cell culture process and are more suitable for the large-scale production of nanoparticles (Sharma et al., 2016). The ability of algae to accumulate metals and reduce metal ions in the biosynthesis of nanoparticles makes them a superior contender for the preparation of nanoparticles (Mukherjee et al., 2019). Metal nanoparticle synthesis by using algae have been reported in the literature (Sahayaraj et al., 2012; Chandran et al., 2016, Azizi et al., 2013; Mahdavi et al., 2013; El-Kassas et al., 2016; Subhashini et al., 2018; Ercan et al., 2019). Using algae in the production of nanoparticles is a promising innovation approach since algae are rich in functional groups such as amino, hydroxyl, and carboxyl groups all of which are responsible for the production of metal nanoparticles (Subhashini et al., 2018; Fawcett et al., 2017; Yew et al., 2016). It has been recently reported that algae are a modern alternative bioagent for the production of iron oxide nanoparticles (Abdul Salam et al., 2012) and their use have become widespread (Mahdavi et al., 2013).

The discharge of industrial wastewater containing dyestuff and metal ions into the environment causes significant problems for all living being including humans (Ibrahim et al., 2009). Congo red (CR) is a water-soluble diazo dye and used in the laboratory to test for free hydrochloric acid in stomach content, in the diagnosis of amyloidosis, as a pH indicator, and also as a histological stain for amyloid. It has a strong affinity for cellulosic fibers and is therefore used in the textile industry. It is considered toxic because it is metabolized to benzidine which is a carcinogenic substance for humans and causes allergic reactions (Chatterjee et al., 2010). Azo dyes pose a threat to aquatic organisms as well as humans (Kumar et al., 2009). Increased GST (glutathione s-transferase) activities in the gills of Tilapia are the result of prolonged exposure to Red 195 dye (Ayadi et al., 2015). It has been reported that CR exposure to aquatic *A. leptodactylus* (Aksu et al., 2017) and *G. pulex* (Tatar et al., 2019) caused unwelcome changes in antioxidant parameters.

Numerous methods are used to remove dyestuffs from the environment. The adsorption process is one of the methods used for the removal of acidic, basic, and neutral dyes from wastewater. The adsorption process has the lowest operating cost and is the easiest to operate among the other methods (Gautam et al., 2013). Besides these favorable properties, the cost of adsorbents and their non-toxicity are important properties as well (Srilakshmi et al., 2016; Mingyan et al., 2021).

A number of studies have been carried out on the use of algae as adsorbent substances (Kousha et al., 2012; Pugazhendhi et al., 2019). Algae are potential and suitable biosorbents owing to their rapid and easy growth, being nontoxic, and containing abundant functional groups. Algae are used in scientific studies in the production of nanoparticles due to their high metal and dye adsorbing abilities rising their rich functional groups. Such as *Padina pavonica* (Phaeophyceae), commonly known as peacock's tail, is a brown alga common in the Mediterranean (Cormaci et al., 2012). It is rich in carbohydrates (mainly alginates and laminarans), lipids (fucosterol), vitamins, and mineral salts (Omezzine et al., 2009; Caf et al., 2015).

Nanoparticles, on the other hand, could be used in various applications including adsorbing and in particular dye retention because of their large surface area, their nanoscale size, increase in the number and surface area per unit area, and the properties of the bio compounds they carry (Ponnuchamy & Jacob, 2016).

The current study evaluated the neurotoxic and antioxidant activity of the nanoparticle by considering the characterization of the nanoparticle, its effectiveness in dye removal at different temperatures, isotherm modeling studies, and the side effects that may occur in nature while removing the CR dye from the wastewater treatment system.

The aim of this study was to synthesize a new surface-modified super magnetic Fe_3O_4 iron nanoparticle (Pa@FeNP) from *Padina pavonica* by employing the green synthesis method. Effects of synthesized Pa@FeNP on aquatic system pollution removal, the purification efficiency of hazardous anionic CR (congo red) dye from aqueous media on different parameters such as pH, temperature, and initial dye concentration were evaluated. Moreover, optimum usage conditions such as dye concentration, initial adsorbent dose, and determination of adsorption isotherm were studied as well. Furthermore, the neurotoxic effect on the SH-SY5Y (Human neuroblastoma) cells and antioxidant activities in vitro were studied with consideration of this nanoparticle will be released into the water system, on the end consumer human.

Material and Methods

Materials

Iron (II) chloride tetrahydrate ($FeCl_2.4H_2O$, Merk 99% purity), iron (III) chloride hexahydrate ($FeCl_3.6H_2O$, Merk 99% purity), (H_2O_2, Merck 64271), sodium hydroxide (NaOH), hydrogen chloride (HCl), Congo Red ($C_{32}H_{22}N_6Na_2O_6S_2$), ethanol ($C_2H_5OH$), methanol ($CH_3OH$), and hydrogen peroxide were obtained from Sigma. Distilled water was used to prepare aqueous solutions.

Preparation of *Padina pavonica* Extract

Padina pavonica (L) was collected from Ornek Village beach on the Mediterranean coast of Antalya from its natural environment. The collected algae were first washed with tap water to remove any pollutants on the algae. The algae were then washed several times

with distilled water and left to dry in the dark for 4 days. Algae extract was prepared by the method described by El Kassas et al. (2016). After washing and drying, 1 g of *P. pavonica* was pulverized, mixed with 100 ml of 100°C distilled water (dH_2O) and infused for 60 minutes. The *P. pavonica* aqueous extract was then cooled to room temperature. The cooled *P. pavonica* extract was filtered to separate the macromolecules used in the synthesis of iron nanoparticles.

Synthesis of Iron Nanoparticle (Pa@FeNPs)

Iron nanoparticles were synthesized by employing green synthesis method in which *P. pavonica* aqueous extract was used as a reducing and capping agent. Accordingly, 0.1 M 50 mL $FeCl_3$ and 0.1 M 50 mL $FeCl_2$ solutions were mixed and 100 mL algae extract (1:1 vol) was added at 70-80°C. Then, 30 mL of 2M NaOH solution was added dropwise for the formation of the nanoparticle, and the colour of yellow ferric chloride solution turned into a black solution with nanoparticle synthesis in a short time. The formation of the nanoparticles was observed with the appearance of the dense black precipitate. The iron nanoparticles were then centrifuged in distilled water at 4500 rpm for 10 min. The particles obtained at the end of centrifugation were washed two times with distilled water and then with ethanol. They were left to dry in the oven at 40°C for 48 hours.

Pa@FeNPs Characterization

After synthesis of Pa@FeNPs, the nanoparticles were characterized using various techniques. Scanning electron microscopy (SEM) images were obtained using a JEOL JSM 6510 at 5 kV in high vacuum mode to determine the morphology of the prepared nanoparticle. Elemental composition analysis was performed using an energy-dispersive X-ray spectroscopy (EDX) analyzer mounted on the Hitachi S-800. Fourier-transform infrared (FT-IR) spectra were used for the determination of functional groups and their possible participation in Pa@FeNP synthesis using the dried pellet method for algae powder and Pa@FeNPs were in the range of 4000 to 400 cm^{-1} (Perkin Elmer Spectrum 100).

An X-Ray Diffraction Spectrometer (XRD) (RIGAKU ULTIMA IV) was used to determine crystallite size and identity. Size range of the particles was determined by Zetasizer (Malvern Zetasizer Nano ZSP). This device allows measuring the dispersion range and zeta potential of the particles. The morphology, size distribution, and particle size analysis of the nanoparticle were carried out using Hitachi HighTech HT7700 Transmission Electron Microscopy (TEM) at 120 kV. TEM samples were prepared using ultra-fine carbon type-A 400 mesh copper grids. Average particle size diameter was calculated from individual particles using the TEM images.

Cell Viability Test

SH-SY5Y (Human neuroblastoma cell line) cells were obtained from Bingöl University, Department of Molecular Biology and Genetics. Normal neuroblast cells maintained at -80°C were grown in DMEM growth medium, passaged every 2 or 3 days at 37°C in a 5% CO_2 oven.

Cell Viability Test of Iron Oxide Nanoparticle

Neurotoxicity effects of Pa@FeNPs on SH-SY5Y cells were assessed by 3-(4,5- dimethylthiazol-2-yl)-2,5 diphenyl tetrazolium bromide (MTT) assay. SH-SY5Y cells were grown to sufficient numbers in 25 cm^2 cell culture flasks at 37°C in a 5% CO_2 incubator. After adding 100 µl of cells to each well, the cells were incubated for 48 hours to proliferate in a 5% CO_2 incubator. One mg of each sample to be tested was weighed and the desired concentration was prepared by dissolving in 1 ml of RPMI 1640 medium in a 1.5 mL eppendorf tube. SH-SY5Y was incubated for 48 hours in a 5% CO_2 incubator with nanoparticle added medium, and the samples were expected to affect the cells and incubated for 72 hours. After 72 hours, 15 µL of MTT substance was added to each well. Cells were incubated at 37°C for 4 hours in a 5% CO_2 incubator. After 4 hours of incubation, absorbance values at 450-690 nm were measured.

Antioxidant Activity Assay

To remove the DPPH radical effect, 50 µL of *P. pavonica* aqueous extract and Pa@FeNPs were collected respectively, and transferred to 96 plate wells. It was vortexed by adding 200 µL of DPPH solution to each well. Then incubated in a dark at room temperature for 60 min. After incubation, absorbance was read in ELISA at 517 nm wavelength. Butylated hydroxyanisole (BHA) was used as a reference antioxidant (Hatano et al., 1988). For metal chelating activity, 5 mM ferrozine solution, and 2 mM $FeCl_2$ solution were prepared. 50 µl of *P. pavonica* aqueous extract and Pa@FeNPs (prepared as 1 mg/mL) was collected respectively, and transferred to 96 plate wells. It was vortexed by adding 160 µl of distilled water and 5 µL of $FeCl_2$ (2 mM) solution to it. After 30 seconds, 20 µl of ferrozine (5 mM) was added and mixed. Absorbances were read at 562 nm after incubation at room temperature for 10 minutes. EDTA (Ethylene diamine tetra acetic acid) was used as a reference antioxidant (Wenli et al., 2004).

Anionic Congo Red (CR) Dye Removal Studies

Adsorption studies of CR (congo red) dye were carried out by using the Pa@FeNPs. In CR adsorption, the effects of initial pH, initial dye concentration, adsorbent amount, and adsorption temperature (25°C and 40°C) were investigated. After the adsorption

process, the dye concentrations in the solution were determined with the SpectraMax Plus384 plate reader.

In dye removal studies by adsorption, initially, effects of pH were examined. CR dye (C.I name=Direct Red 28, C.I No.=22120, Chemical formula= $C_{32}H_{22}N_6O_6S_2Na_2$, Formula weight=696.65) was prepared separately with distilled water at room temperature. Then, 9 ml CR dye was added to 7 vials of 50 ml in the desired ppm from the prepared stocks. Similarly, 9 ml CR dye was added to 7 vials. The pH of each solution was adjusted in the range of 2-8. Separately, 10.0% H_2O_2 solution (v/v) was prepared by diluting 30.0% H_2O_2 solution with deionized water. Then, 1 ml H_2O_2 (10.0%) was added to each dye sample and 200 µl samples were taken for the initial dye concentration, transferred to a 96-plate, and measured at 538 nm in the ELISA reader. Pa@FeNPs (15 mg) were added to 7 vials. Then, pH 2-8 solutions prepared with CR were transferred to bottles. The solutions were sampled every half hour for 3 hours at 200 rpm in a shaker and the measurement was made in the ELISA device. After determining at which pH the best dye removal was found, dye removal at different ppm was examined. These processes were carried out at 25°C and 40°C.

After determining the pH with the highest percentage of dye removal, CR dye removal at 20 mg/L, 50 mg/L, 100 mg/L, and 200 mg/L using 5 mg, 10 mg, 15 mg, and 20 mg NPs was investigated. The experiment was completed using the same conditions.

Adsorption Isotherm

Adsorption isotherm is graphed expressing the equilibrium state between the amount of substance adsorbed on the adsorbent (qe, mg g^{-1}) and the remaining substance concentration in the solution (Ce, mg L^{-1}) at constant temperature and pH. These isotherms can be obtained by equilibrating solutions prepared at different concentrations with a known amount of adsorber. The equations commonly used to describe the adsorption isotherm are the Langmuir, Freundlich, and Temkin equations. With the aid of these equations, the surface properties of the adsorbent and the relationship between adsorbent and adsorbed can be defined.

The Langmuir isotherm model (Equation 1) assumes that adsorption takes place on a homogeneous surface and in a monolayer. Additionally, Langmuir acknowledges that all active sites have the same energy and equal affinity for the molecules to be adsorbed. The adsorption capacity (qe) and removal efficiency of the biosorbent at equilibrium were determined using Eqs. (1) and (2), respectively:

(1) $qe=\frac{Ci-Ce}{W}\times V$

(2) Adsorption (% removal efficiency)$=\frac{Ci-Ce}{Ci}\times 100$

Adsorption isotherms were applied to explain the equilibrium adsorption characteristics. Eq. (3) represents Langmuir's isotherm.

$$(3)\ q_e = \frac{q_{max}K_L C_e}{1+K_L C_e}$$

Langmuir's isotherm was transformed into its linear form, as represented in Eq. (4), to determine the adsorption parameters.

$$(4)\ \frac{1}{q_e} = \frac{1}{K_L q_{max}} . \frac{1}{C_e} + \frac{1}{q_{max}}$$

Here, q_{max} represents the maximum adsorption capacity (mg/g) and K_L (L/mg) is the Langmuir isotherm constant which indicates the binding affinity between Pa@FeNPs and CR.

The separation factor (R_L) was calculated using the following equation.

$$(5)\ R_L = \frac{1}{1+C_i \times K_L}$$

where R_L is the dimensionless Langmuir constant indicating the probability of positive ($0<R_L>1$), negative ($R_L>1$), linear ($R_L = 1$), or irreversible ($R_L = 0$) adsorption.

The Freundlich isotherm model assumes that adsorption is multilayered. It also recognizes that the adsorber surface is heterogeneous in terms of adsorption areas and energy. Equation (6) represents Freundlich's isotherm.

$$(6)\ q_e = K_f C_e^{\frac{1}{n}}$$

The linear form of the Freundlich isotherm is shown in Equation 7.

$$(7)\ \mathrm{Log}\, q_e = \mathrm{Log}\, K_f + \frac{1}{n}\mathrm{Log}\, C_e$$

Here, K_f is the Freundlich constant and is used to measure the adsorption capacity and 1/n is the adsorption density. A value of 1/n indicates that the adsorption process is either positive ($0.1<1/n<0.5$) or negative ($1/n>2$).

According to the Temkin isotherm, the decrease in the heat of adsorption of all molecules occurs in a linear order. This indicates that the binding energy is homogeneous (Temkin and Pyzhev, 1940). The equation expressing the Temkin isotherm is given below.

$$q_e = \frac{RT}{b} lnK_T C_e$$

$$q_e = \frac{RT}{b} lnK_T + \frac{RT}{b} lnC_e$$

$$q_e = B_T lnK_T + B_T lnC_e$$

Here, B_T=RT/b. b is the Temkin isotherm constant and K_T is the equilibrium binding constant (Lg-1).

Adsorption Kinetics

For dye removal, the adsorption rate was analyzed using pseudo-first-order and pseudo-second-order kinetic models. It is represented by the pseudo-first-order equation:

$$(8)\ \ln(qe\text{-}qt) = \ln qe - K_1 t$$

where qt represents the adsorption capacity (mg/g) at time t while K_1 (min^{-1}) is the equilibrium rate constant.

The so-called quadratic equation is represented by (9).

$$(9)\ \frac{t}{q_e} = \frac{1}{K_2 q_e^2} + \frac{1}{q_e}$$

Here, K_2 (g mg^{-1} min^{-1}) is the equilibrium ratio constant. The linear regression coefficient (R^2) values are used to predict the most suitable isotherm and kinetic model for the adsorption process.

Thermodynamic Parameters

Thermodynamic considerations are necessary to determine whether the adsorption process is spontaneous or not. To determine the thermodynamic parameters of adsorption and the adsorption behavior, thermodynamic analyzes were carried out at two different temperatures, 25°C and 40°C.

In the adsorption study of Pa@FeNPs and CR dyestuff, the activation energy was calculated with the Arrhenius equation given in Equation 10

$$(10)\ Lnk_2 = LnA - \frac{E_a}{RT}$$

Gibbs free energy change (ΔG°, kJ/mol), enthalpy change (ΔH°, kJ/mol), and entropy change (ΔS°, kJ/mol) were calculated using equations 11, 12, and 13

$$(11)\ \Delta G^\circ = -RTLnK_c$$

$$(12)\ K_c \frac{\text{The amount of dye adsorbed (mg/L)}}{\text{The amount of substance that remained in the solution (mg/L)}}$$

$$(13)\ \Delta G^\circ = \Delta H^\circ - T\Delta S^\circ$$

Statistical Analysis

All measurements were made in triplicate. One-way ANOVA was used in the analyzes and GraphPad Prism 8.0.3 software was used for plotting. Multiple post-hoc comparisons were made for two or more groups using Dunnett's multiple comparison tests. Statistical significance was expressed at $p<0.05$

Results and Discussion

Pa@FeNPs Characterization:

Algae extracts can act as reducing and capping agents in the bioreduction reactions for the synthesis of metallic nanoparticles due to their rich secondary metabolite contents The current study focused on green synthesis of iron nanoparticles by *P. pavonica* (Pa@FeNPs) and removal activity of anionic azo dye congo red (CR). Congo red removal efficiency of 95% was obtained by using Pa@FeNPs. The surface areas of iron and iron oxide nanoparticles are much larger than the surface areas of micro-sized metal particles. Therefore, iron and iron oxide nano-sized materials are effective for cleaning pollutants. In this manner, seaweeds are of great importance in the synthesis of metal oxides and constitute an important aspect of this research (Fawcett et al., 2017). There are many nanoparticle studies on marine seaweed with different metals (Azizi et al., 2014; El-Kassas et al., 2016; Subhashini et al., 2018; Abboud et al., 2014; Khanehzaei et al., 2014; Francavilla et al., 2014; Salem et al., 2019). Seaweed, which has a rich content in functional groups, can act as a good stabilizer and coating agent in the synthesis of iron nanoparticles. It is stated that approximately 2,500 bioactive compounds are isolated from the sea and 93% of these components are obtained from marine seaweed (Kardono, 2004.) These phytochemicals consist of simple molecules such as phenolic acids or flavonoids, to highly complex polymers, a subgroup of tannins formed by the polymerization of phloroglucinol units called phlorotannins (Mekini´c et al., 2019; Cotas et al., 20209. Marine algae have been reported to be a rich source of catechin, rutin, quercetin, hesperidin, and other flavonoids (Cotas et al., 2020). *Padina pavonica*, a brown algae, also contains flavonoids such as resveratrol, myricetin, morin, quercetin, naringenin, and resveratrol (Caf et al., 2015). Seaweed, which has a rich content in functional groups, can act as a good stabilizer and coating agent in the synthesis of iron nanoparticles.

In the current study, iron nanoparticles synthesized by the biosynthesis method were used as an adsorbent in the adsorption process and the synthesis of nanoparticles was carried out using *Padina pavonica*, a marine macroalgae, as a biological reducing agent. The formation of iron nanoparticles was first observed when the water extract from *P. pavonica* was added to the iron solution, turning the clear solution color to black. The color of the solution turned black due to the formation of Fe_3O_4 nanoparticles. This chemical process is a result of the surface resonance phenomenon with the reduction of Fe^{+2} to Fe^0 and the formation of Fe_2O_3.

The UV-Vis spectrum of Pa@FeNPs nanoparticles (Figure 1) shows an absorption band in the 325 and 375-nm region. This is due primarily to the absorption and scattering of UV radiation by magnetic nanoparticles, which is in accordance with the some literature (ur Rahman et al., 2012; El Kassas et al., 2016). This result

fully matches the UV-Vis spectra of nanoparticles prepared using *K. alvarezii* seaweed extract (Yew et al., 2016; Anjana et al., 2018). This may be due to the phytocompounds such as tannins, phenols, alkaloids, flavonoids and saponins content of the *P. pavonica.* The functional groups and polysaccharides of seaweed are strong stabilizers that provide biocompatibility and chemical functionality to nanostructures (Dias et al., 2011; (Herrera-Becerra et al., 2010).

To determine the functional groups contained in the adsorbent used in the dye removal study, FT-IR analyzes were performed before adsorption and the corresponding spectra are shown in Figure 2. The functional groups contained in the adsorbent were studied at 650–4000 cm^{-1}. Sulfated polysaccharides obtained from seaweed have a strong ability to synthesize nanoparticles. Therefore, the sulfate group may be responsible for the reduction of iron ions by oxidation of aldehyde groups to carboxylic acids (Mahdavi et al., 2013). The spectra of the *P. pavonica* extract showed strong absorption bands at 3267, 1440, 1067, 863, 719 and 617 cm^{-1}. When we look at the spectra of Pa@FeNPs, it is seen that the peak hydroxyl groups are at 3402 cm^{-1}, the peak methylene groups at 2934 and the amino groups at 1650 cm^{-1} which may be responsible for the reduction. (Figure 3). These peaks indicated the presence of sulfated polysaccharides and aromatic rings in *P. pavonica*. Therefore, *P. pavonica* extract containing sulfate, hydroxyl, and aldehyde groups may be responsible for the reduction of Fe^{3+} and the synthesis of Pa@FeNPs (Iram et al., 2010). These peaks in FT-IR also indicate the presence of phenolic acids and flavones in the extract, which enables the reduction of metal ions and the formation of nanoparticles (Amini & Akbari, 2019).

Surface morphology, particle shape and size images of SEM analyzes are given in Figure 3. Nanoparticles showed a polydisperse distribution in SEM and surface porosity allowing free passage of dye molecules.

EDX analyses were performed to determine the contents of adsorbents of synthesized iron nanoparticles (Figure 4). In the study, the composition and mapping of the elements on the surface of the

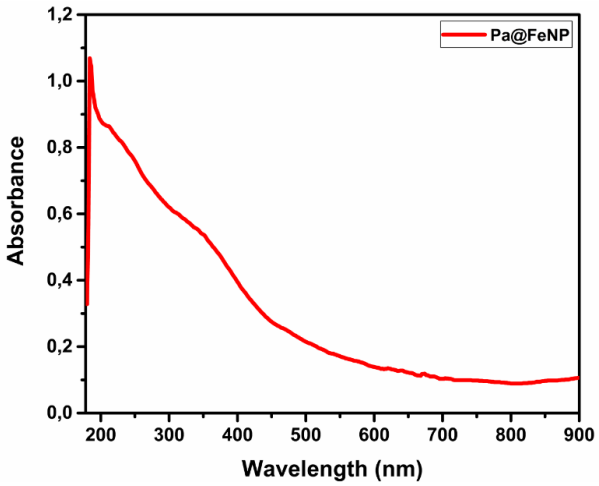

Figure 1. UV-Vis absorption spectrum of synthesized Pa@FeNPs

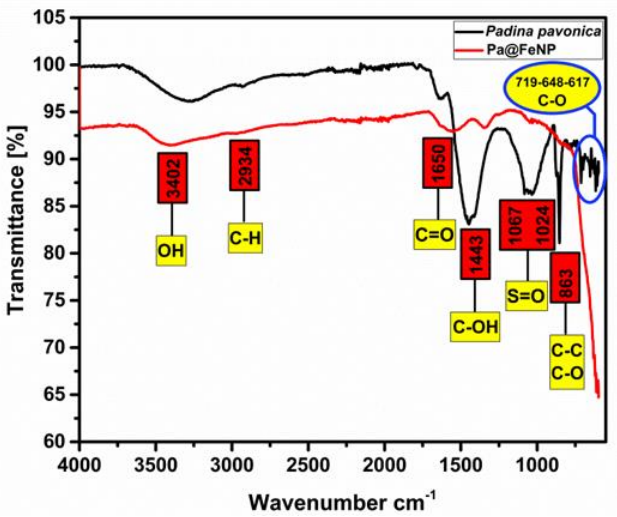

Figure 2. Infrared spectrum of Pa@FeNPs synthesized using *P. pavonica* (Linnaeus) aqueous extract

nanoparticle was carried out. When we look at the results, the presence of peaks showing the binding energies of prominent iron and oxygen atoms confirms that Pa@FeNPs biosynthesis has taken place (Figure 4b). The peaks of the Cl element from ferric chloride, which is used in the biosynthesis of iron nanoparticles, have been seen in many studies and are an indication that the nanoparticles are not washed well (Qasim et al., 2020). In the EDX data, weak peaks from elements such as carbon, nitrogen, sulfur may be due to phytochemicals from the extract.

The crystal structure and phase identification of Pa@FeNPs were characterized by XRD as given in Figure 5. In XRD analysis performed at 2θ scale, Pa@FeNPs gave characteristic peaks at 23°, 38°, 54.9°, 60.3° and 68.8°. It was determined that the obtained peaks are characteristic peaks belonging to magnetite. The indices corresponding to these peaks, respectively, are (111), (220), (400), (331), and (422). The result of the XRD analysis confirms the synthesis of magnetite nanoparticles. These are the peaks of the crystalline iron oxide, and these peaks are the magnetite (Fe_3O_4) form of the synthesized nanoparticles. This fits the reference model for Pa@FeNPs (JCPDS: 01-074-1910/Cubic). The presence of a large peak representing XRD iron nanoparticles indicates that the synthesized iron nanoparticle crystals are small or structurally irregular. The weak characteristic peak values in XRD analysis show that the iron nanoparticles are in an amorphous structure. These results agree with the iron oxide nanoparticle previously obtained by green synthesis (Okath, 2016).

Structural and morphological forms of the Pa@FeNPs were investigated using TEM. The thin layer surrounding Pa@FeNPs supports the presence of plant metabolites found in the water extract of *P. pavonica* that reduce Fe ions to nanoparticle. The TEM image of Pa@FeNPs (Figure 6) showed that the nanoparticles were spherical but also agglomerated. This can be attributed to the thickening property of *P. pavonica*, a

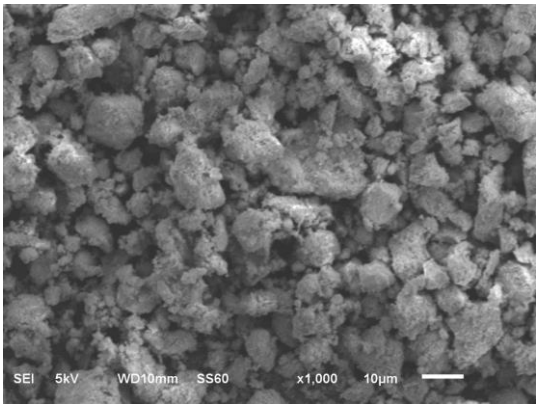

Figure 3. SEM image of Pa@FeNPs

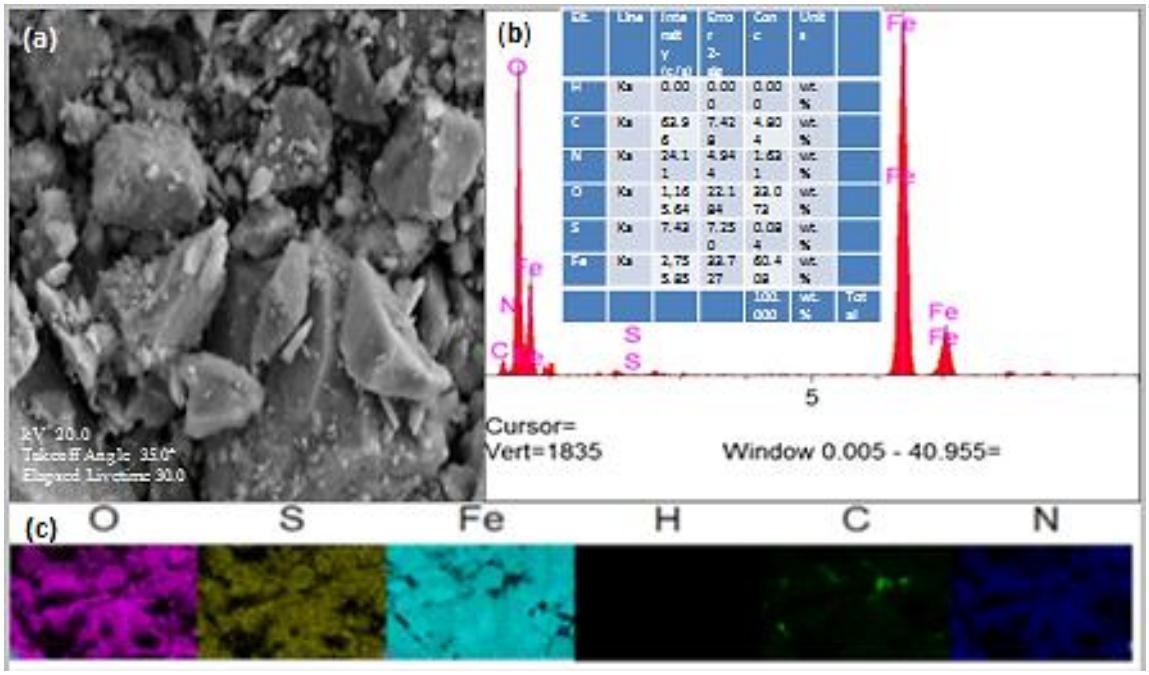

Figure 4. EDX image of Pa@FeNPs **(a),** SEM micrograph of elemental compositions and EDX profile **(b)** EDX mapping of elements Fe, O, S, H, C and N in Pa@FeNPs **(c)**

brown alga. It is also a phenomenon observed when the nanoparticle is magnetic and has a small size (Yew et al., 2016). The size of the nanoparticle was measured as 10.53 -20.55 nm in the size distribution histogram. In this study, results are somewhat similar to the sizes of iron oxide nanoparticles (22-33 nm) prepared with *Jania rubens* was obtained. (Salem et al., 2020). It has been reported that the mean diameter of the iron oxide nanoparticle obtained by the green synthesis method from the brown seaweed *Sargassum muticum* is 18 ± 4 nm (Mahdavi et al., 2013). The electrical charge of the Pa@FeNPs obtained by the green synthesis method was determined by DLS. Zeta potential, a measure for determining the charge on the surface of nanoparticles, indicates the electrical potential of sliding of nanoparticles. The electrical charge of the Pa@FeNP was −8.53 mV as a result of zeta potential analysis (Figure 7). In plant-based biosynthesis studies, zeta potential distributions were found to be negative (Oliveira et al., 2019; Dubeyet al., 2013). Iron nanoparticles show a negative value due to the adhesion of organic compounds to the surface of the iron nanoparticles (Singh et al., 2020). Nanoparticles with negative zeta potential exhibit agglomerated structures. This is observed in the SEM micrograph. In this study, the source of the negative Zeta potential for Pa@FeNPs may be due to the chemical components of the reducing and sealing agent used in the green synthesis, as well as the particle size of the nanoparticle.

Fenton–Like Catalytic Activity for the Degradation of CR (Congo Red) Dye

In the present study, H_20_2 was used as a Fenton-like catalyst. Currently, this mechanism, in which the Fe^0/H_2O_2 system functions, has been used most commonly (Xu & Wang, 2011). In a study for dye removal at different concentrations using biologically synthesized iron nanoparticles in the presence of H_20_2, dye removal was found to be high at all concentrations (Shahwan et al., 2011). Similar results were obtained in our study. Electron transfer between ferric ions and ferrous ions imparted unique electromagnetic properties to Fe_3O_4, and Fe_3O_4 enhanced the removal effect of the congo red dye by participating in the Fenton-like reaction through the liberation of structural

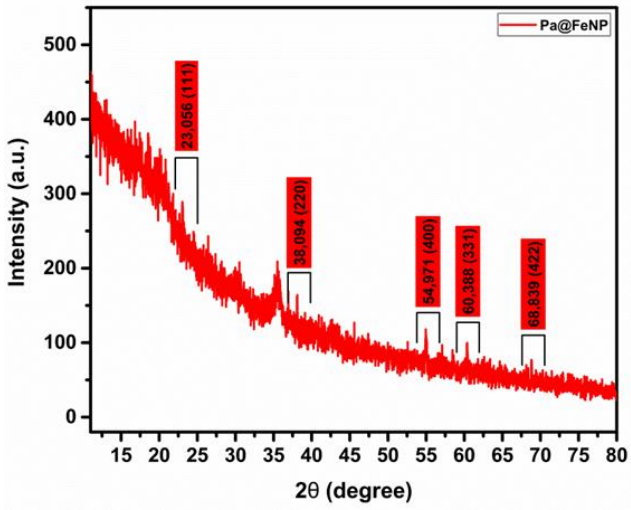

Figure 5. XRD pattern of synthesized Pa@FeNPs.

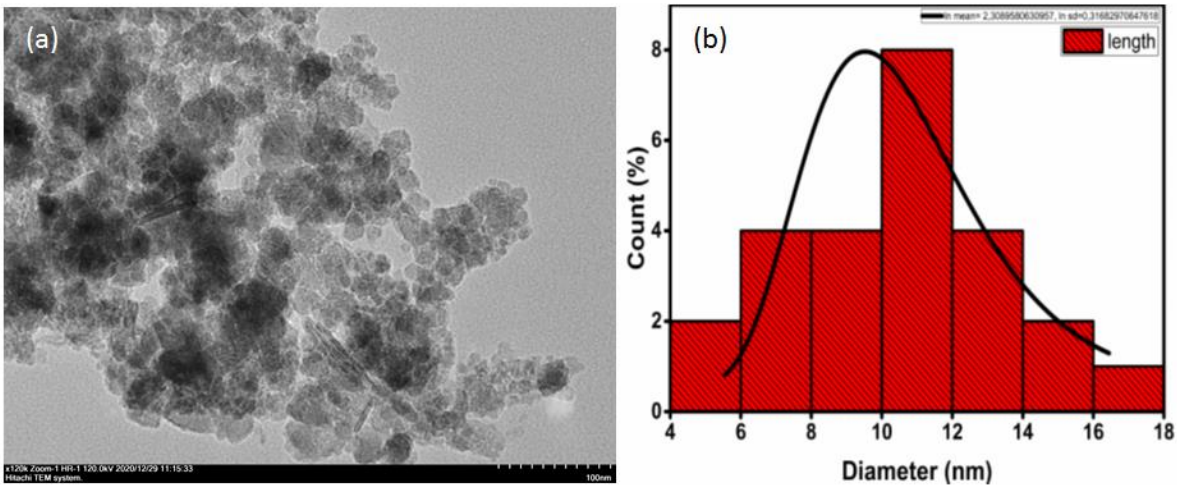

Figure 6. TEM image (a) and particle size histogram distribution plot of Pa@FeNPs (b)

Fe^{2+}/Fe^{3+}, facilitating the decomposition of H_2O_2. Flavonoids have a direct effect on Fe^{3+} ion concentrations and reduce Fe^{3+} to more Fe nanoparticles. At the same time, flavonoids prevent oxidation of the nanoparticle surface. A more effective dye removal is provided in the presence of H_2O_2 under acidic conditions. In studies with Fenton, the most suitable dye removal and the highest production of H_2O_2 are in acidic conditions (Xiaofan et al., 2020). The optimum pH was around 4 in the presence of Fenton's reagent. In addition, a high pH can significantly reduce the degradation efficiency of target pollutants (Rivas et al., 2001).

The relationship between the percentages of dye removal over time at various initial dye concentrations is shown in Figure 7. As the dye concentration increased from 20 mg/L to 200 mg/L, CR dye removal decreased from 74.04% to 47.61% at 25°C. This result was associated with a decrease in the surface area and binding sites of the biosorbent. In general, the rate of adsorption is strongly influenced by several parameters, including the state of the solid, the availability of solute, and the position between reactive binding sites (Cengiz & Cavas, 2008). The pH is important in the adsorption process since it affects the surface charges of dyes and adsorbent materials, the degree of ionization of functional groups, and the adsorption mechanism (Elmoubarki et al., 2015). In the present research, the pH was studied in the range of 2-8 as given in Figure 9 and 10. CR is a dipolar molecule that exists in the anionic form at basic pH and cationic form at acidic pH. Hou et al. (2012) have reported that CR dye is an anionic dye, and since its surface will be negatively charged in the pH 6-8 range, the dye removal is high in this pH range.

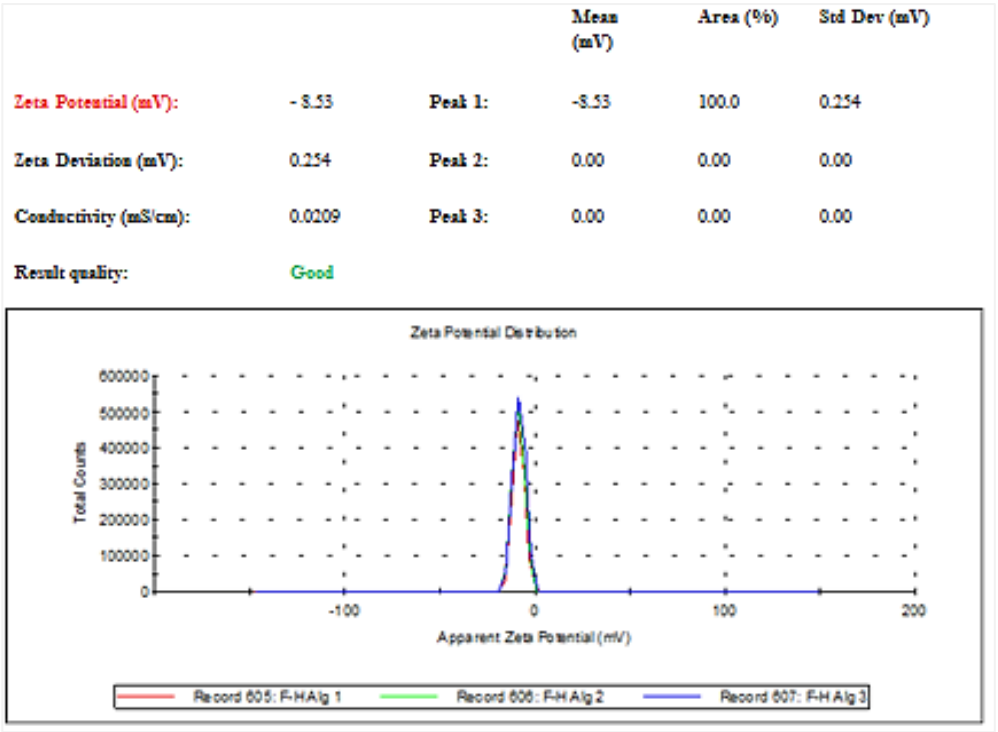

Figure 7. Zeta potential plot of Pa@FeNPs.

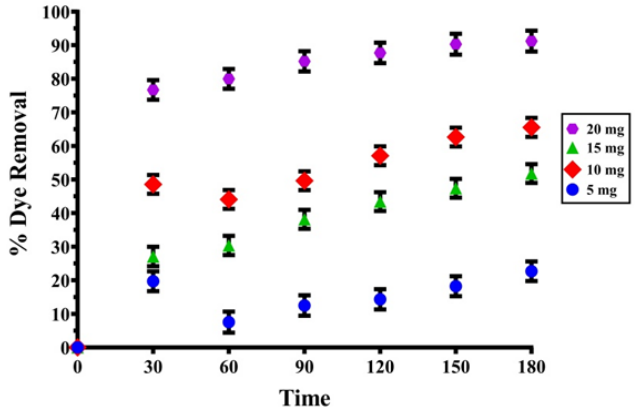

Figure 8. Congo red dye removal at 25°C using 50 ppm dye concentration at 5-20 mg Pa@FeNPs.

However, in our study, the best results for CR dye were obtained in an acidic environment (40°C, pH: 4, 95%). According to the zeta potential analysis, the surface of the Pa@FeNPs is negatively charged (Figure 7). At acidic pH, the dye molecules exist as cations and therefore the adsorption of CR on the surface of the Pa@FeNPs is much higher at an acidic pH. As the pH of the system increases, the number of negatively charged sites increases and the number of positively charged sites decreases. A negatively charged surface region on the adsorbent does not support the adsorption of dye anions due to electrostatic repulsion (Bhoi, 2010). Bhoi (2010), reports that the adsorption of CR on the PAC and GAC surface is much higher at acidic pH.

CR removal activity was studied at 2 different temperatures (25 and 40°C) using different amounts of Pa@FeNPs per 10 ml solution. As shown in the figure below, the adsorption percent capacity of the Pa@FeNPs increased with the rise in temperature. At 25°C, dye removal was observed in all pH ranges, however, the highest percent removal was observed at pH 4. At 40°C, the highest percentage removal was observed at pH 4. The removal percentage decreased as the dye concentration increased. This may be due to the decrease in the unit removal efficiency of the dyestuff when the dye concentration per unit of surfactant increases. As the dyestuff concentration increases, the percentage of dyestuff removed with the Pa@FeNPs decreases. Similar results have been observed in other studies (Prasad et al., 2017).

Pa@FeNPs were studied in the range of 0.005-0.020 g for dye degradation (Figure 8, 10). From an economic point of view, it is important to select the appropriate adsorbent concentration for industrial applications. The percentage removal was 25.99% with 0.005 g adsorbent in the medium with 50 mg/L CR and the removal increased to 93.18% when the adsorbent dose was increased to 0.020 g. The increase in this removal was associated with a large number of active sites on the adsorbent surface and an increase in the adsorbent dose.

Different contact times (30-180 min) were applied to observe the CR dye removal capabilities of the Pa@FeNPs. Adsorption time is a condition that affects

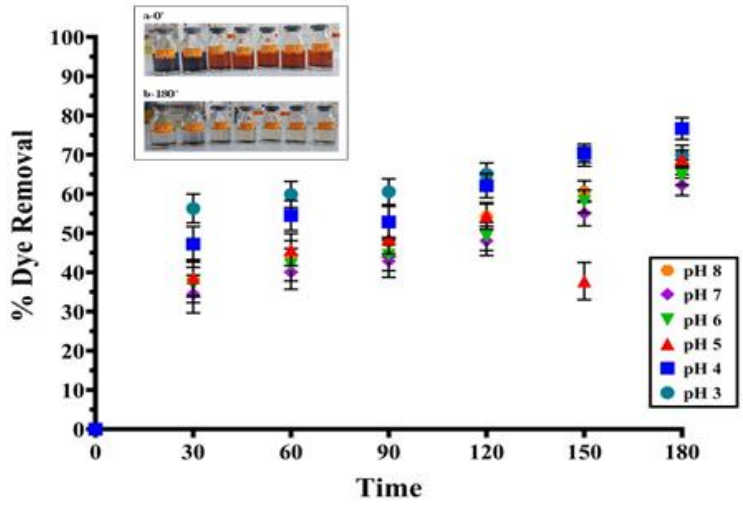

Figure 9. Congo red dye removal at various pH values at 25°C and 20 ppm dye concentration with 15 mg Pa@FeNPs (a: initial: 0'; b: 180').

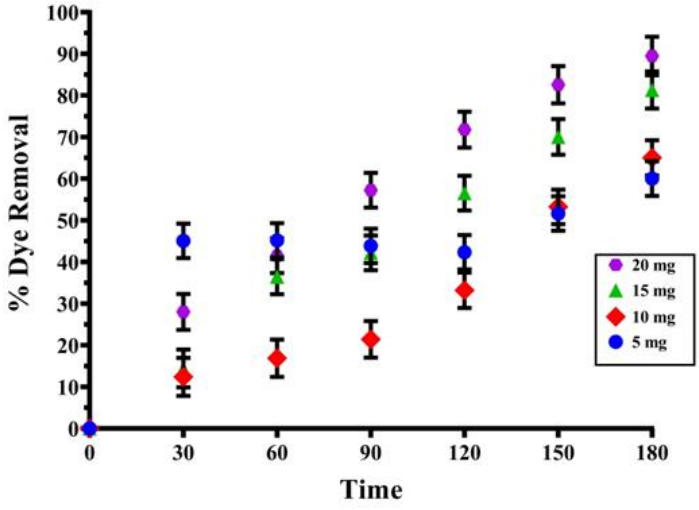

Figure 10. Congo red dye removal at 40°C with 50 ppm dye concentration at 5 mg, 10 mg, 15 mg, and and 20 mg Pa@FeNPs.

the percentage of dye removal of the nanoparticle, and the most effective removal time for the Pa@FeNPs was 150 min. (Figure 8-11).

The Pa@FeNPs were studied for dye degradation at 25°C and 40°C. In the presence of CR dye, a better dye percent removal was observed at 40°C (Figure 11). It has been suggested that the increase in temperature increases the diffusion rate of the adsorbent molecules along the outer boundary layer and in the inner pores of the adsorbent particle, increasing the number of active sites for adsorption and also causing the mobility of the adsorbate molecules (Seki et al., 1998; Chern & Wu, 2008). When we look at the percent dye removal, dye removal and color removal increase as the temperature increases (Luo et al., 2015). However, it was observed that the adsorption capacity decreased as the temperature increased compared to the isotherm Langmuir isotherm. The adsorption capacity of CR on Pa@FeNPs decreased from 86.43 to 41.25 mg g^{-1} as the temperature increased (Table 1). That is, the sorption efficiency was decreased with rising temperature. The tendency of adsorption to decrease with rising temperature in the literature is an indication that adsorption is exothermic, as stated in many studies (Doğan et al., 2009; Vimonses et al., 2009). At the same time, the increase in temperature causes a decrease in the adsorption forces between the active sites on the adsorbent surface and the dye molecules, depending on the decrease in the amount of adsorption (Yagub et al., 2014; Kopaç & Sulu, 2019).

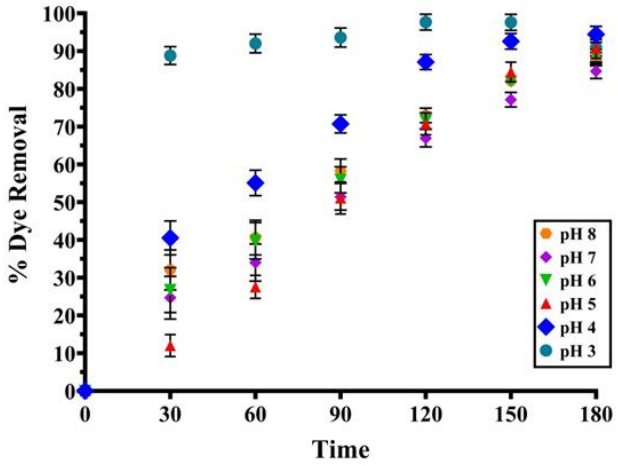

Figure 11. Congo red dye removal at various pH values with 15 mg Pa@FeNPs at 40 °C and 20 ppm dye concentration

Table 1. Isotherm and kinetic parameters of Pa@FeNPs in CR dye removal (50 ppm in the presence of 15 mg adsorbate).

Isotherm model	Isotherm parameters	Temperature (°C)	
		25	40
Langmuir	$qm(mg\ g^{-1})$	86.4304235	41.2541254
	$K_L(L\ mg\text{-}1\ )$	0.007298	0.175627
	R_L	0.73265	0.102236
	R^2	0.99004	0.88709
Freundlich	$Kf\ ((mg\ g^{-1})(L\ mg^{-1})^{1/n}$	1.402523	7.538067
	$1/n$	0.68626	0.4451
	R^2	0.88238	0.97426
Temkin	$B_T(J\ mol^{-1})$	11.4107	12.3241
	$K_T(L\ mg^{-1})$	0.1632	0.808749969
	R^2	0.9336	0.84191
Kinetic model	Kinetic parameters		
Pseudo-first-order	$qe_{exp}(mg/g)$	14.1854	21.36024
	$q_{e\ cal}(mg/g)$	6.813255	10.87156
	$k_1(dk^{-1})$	-0.00017	$-1.3x10^{-4}$
	R^2	0.29652	0.0539
Pseudo-second-order	$q_{e\ cal}(mg/g)$	14.8214	29.985
	$k_2(mg\ g^{-1}\ min^{-1})$	0.004054	$3.6x10^{-4}$
	R^2	0.94353	0.29493

Adsorption, Kinetic and Thermodynamic Parameters

Adsorption isotherms play an important role in explaining how adsorbent and dyestuff molecules interact, giving an idea about the adsorption capacity and understanding the adsorption mechanism. Among the many isotherm models, the Langmuir and Freundlich models are the most commonly used. Langmuir (1918), Freundlich (1906) and Temkin (1940) isotherms have been used for the adsorption of CR dyestuffs. While applying these isotherms, the dyestuff concentration was varied between 5-200 mg/L and the biosorbents were used at 15 mg concentration. Isotherm constants (qm, K_L, K_F, n, aT, and bT) were calculated using the linear form of Langmuir, Freundlich, and Temkin isotherms obtained using experimental adsorption data for CR dyestuff and are given in Table 1. Comparing the biosorbents and dyestuff removal in terms of correlation coefficients (R^2=0.99), Langmuir best described the isotherm model (Figure 12). The data show that the adsorption studies fit the Langmuir Isotherm model. This indicated that the dyestuff biosorption process with biosorbents occurred in a monolayer. The RL value of 0.73, which shows the shape of the isotherm in this model, indicates that the absorption is appropriate and the process is favorable (Mckay et al., 1982) (Table 1). Langmuir isotherm reveals that, in adsorption, all parts of the surface are not covered, there are places where coverings are formed, the adsorption energy is the same on all sides of the surface, and there is no interaction between the molecules attached to the surface (Langmuir, 1918). It shows that the biosorption of CR on *Padina Pavonica* at 25°C fits the Langmuir model best, while the biosorption of CR on *Padina pavonica* at 40°C works well with the Freundlich model as seen in Figure 12.

As a result of the kinetic analyzes carried out to determine the rate of biosorption, it is seen that the biosorption kinetics of the dyestuff used in our study is more compatible with the Pseudo second order kinetic model (R^2=0.94) at 25°C (Figure 13). This shows that the step that controls the rate of adsorption process is the adhesion step to the adsorbent surface. In addition, the maximum adsorption capacity estimated for CR adsorption according to the pseudo-second order kinetic model (qe cal =14.82; qe exp=14.18mg/g) was close to the experimental maximum adsorption capacity (Table 1). Adsorption capacities and kinetic energy models of Congo red with different biosorbents were studied. In this study, the adsorption capacity of the congo dye was found to be 86.43 mg/g as seen in Table 2.

The ΔH^o value was measured as 52.41 KJ mol^{-1}. A value of ΔH^o>0 indicates that this process is endothermic, and a negative value indicates that the adsorption process is appropriate and spontaneous (Figure 14, Table 3). It also shows that the event is chemical adsorption and there is a strong attraction

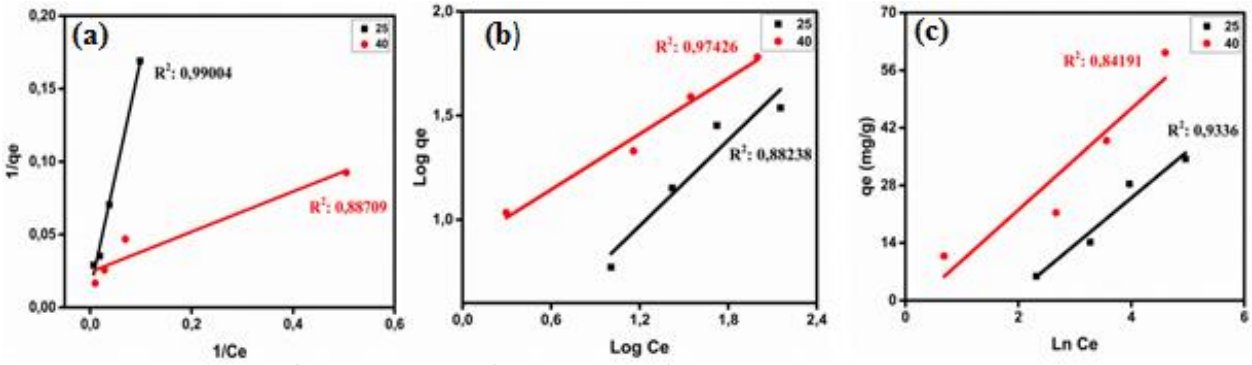

Figure 12. Plots of Langmuir İzotermi Freundlich İzotermi, Temkin İzotermi **(**respectively)

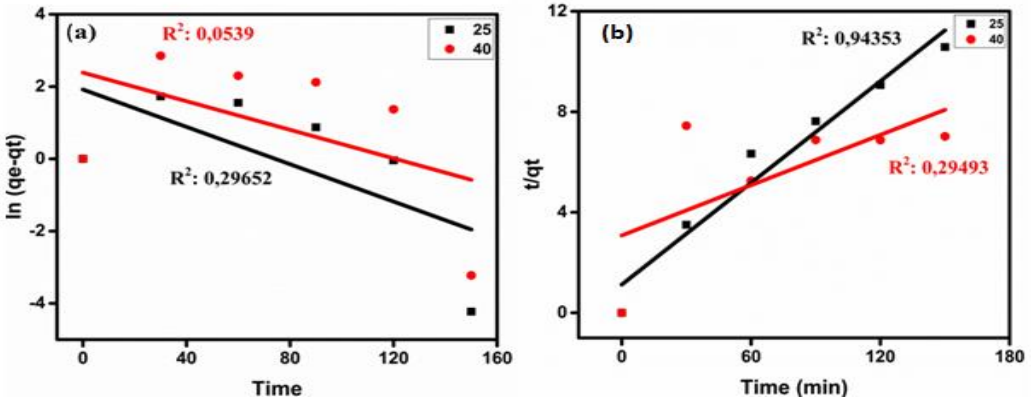

Figure 13. Pseudo-first-order **(a)** and pseudo-second-order **(b)** kinetic models for CR adsorption of the Pa@FeNPs

between the dye and the surface of the adsorbent (Chatterjee et al., 2005). The negative absolute value of ΔG^o (-1.3334 KJ mol^{-1}) indicates that adsorption occurs spontaneously. Absolute value of ΔG^o between -20 KJ mol^{-1} and 0 KJ mol^{-1} indicates that the adsorption process is physical adsorption (Li et al., 2019). Positive ΔS^o values (170.74 KJ^{-1} mol^{-1}) indicate a random increase in the solid/liquid interface during adsorption.

Neurotoxicity and Antioxidant Activity

Interactions between nanomaterials and cells are among the most important issues regarding cellular uptake and subsequent toxic response of the cell. The neurotoxicity effects of Pa@FeNP and *P. pavonica* extract are given in Figure 15. As seen in Figure 15, in the MTT assay, the IC 50 values of *P. pavonica* and Pa@FeNPs were 0.128 and 400 µg/ml for the SH-SY5Y cell lines, respectively. The data for *Padina pavonica* are consistent with previous studies in other cell lines (Deghrigue et al., 2015). Polyphenols, steroids and terpenoids in *P. pavonica* have antiproliferative activities, especially polyphenols act as cancer blocking agents. Diterpenoids in brown algae are also antiproliferative characteristic (Deghrigue et al., 2015). Viability inhibition of various extracts from *P. pavonica* in lung carcinoma cell line, liver carcinoma cell line (Awad et al., 2008), Human oral epidermal cancer cell line cell (Ktari & Guyot, 1999) has been reported. In a different study examining the neurotoxic effect of MgO nanoparticles on the SH-SY5Y cell line, it was shown that there was no significant cell toxicity (Nalci et al., 2020). Pa@FNPs used in this study showed neurotoxicity at a high dose of 400 µg/ml in the SH-SY5Y cell line (Figure 15). The dose and size of nanoparticles play an important role in inducing toxicity. It interacts with NADHP oxidases in the cell membrane and mitochondria of nanoparticles to form superoxide anions. This leads to cytotoxicity by activating redox steps (Radu et al., 2010; Yoonus et al., 2021).

Namvar et al. (2014) evaluated the cytotoxicity, cellular response and anticancer activity of Fe_3O_4

Table 2. Adsorption capacities of Congo red with different biosorbents

Adsorbent	qm (mg/g)	Reference
MFe_2O_4	149.2	(Wang et al., 2012)
iron NPs (ICNPs)	0.032	Ali et al., 2016)
ZnO NPs	71.4	(Kataria et al., 2017)
$FexCO_3$-xO_4	128.6	(Liu et al., 2019)
$CoFe_2O_4$-Chitosan	162.68	(Simonescu et al.,2021)
S. dentifolium (AF-S)	28.24	(Labena et al., 2021)
CSB/ZnONPs	555.6	(Iqbal et al., 2021)
$CoFe_2O_4$ NPs	18.5	(Behura et al., 2021)
Pa@FeNPs	86.43	Present study

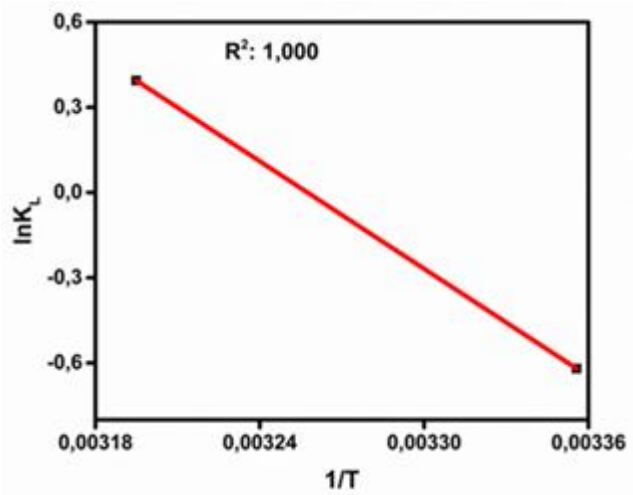

Figure 14. Graph showing the relationship between ln KL and 1/T for CR removal with Pa@FeNP.

Table 3. Thermodynamic parameters for metal/dye (Pa@FeNPs/CR dye) sorption on the adsorbent

Adsorbent	Temp (K/°C)	K_L	ΔG^o (KJ mol^{-1})	ΔH^o (KJ mol^{-1})	ΔS^o (KJ^{-1} mol^{-1})	R^2
Pa@FeNPs	298/25	0.539	-1.3334	52.4160	170.7419	1
	313/40	1.484	-3.8602			

nanoparticles against human cell lines for leukemia, breast cancer, cervical cancer and liver cancer, confirming that the accumulation of Fe_3O_4 nanoparticles in treated cells tends to promote cell apoptosis and their potential use in cancer therapy. It has been reported that magnetic iron oxide nanoparticle obtained from *Sargassum muticum* has cytotoxic effects on different cancer cell lines *in vitro*. Ling et al. (2011), evaluated the efficacy of superparamagnetic iron oxide nanocrystals loaded simultaneously with docetaxel, a chemotherapeutic anticancer drug, and reported that the targeted nanoparticles had an antiproliferative effect in the cytotoxicity study in PC-3 prostate cancer cells.

Antioxidant assessment of Pa@FeNP was examined using DPPH and metal-chelating assays. The results showed strong metal chelating activity compared to the standard (Figure 16a, 16b). The antioxidant potential of both the *P. pavonica* aqueous extract and Pa@FeNPs were revealed by DPPH radical scavenging (Figure 16a) as shown by significant DPPH scavenging activities. The aqueous extract of *P. pavonica* and Pa@FeNPs showed 70.96% and 39.6% DPPH activity, respectively. *P. pavonica* showed radical scavenging activity close to the BHA standard, while Pa@FeNPs showed significantly lower activity ($p < 0.05$). Similarly, Vitta et al. (2020), have reported that FeNP nanoparticles showed lower DPPH activity than the plant extract. The low DPPH radical scavenging potential of Pa@FeNPs can be interpreted as the role of bioactive compounds in reducing and scavenging iron oxide nanoparticle formation. Previous studies show that FeNPs have greater, less, or equal DPPH scavenging capacity compared to the biological extract used in FeNP

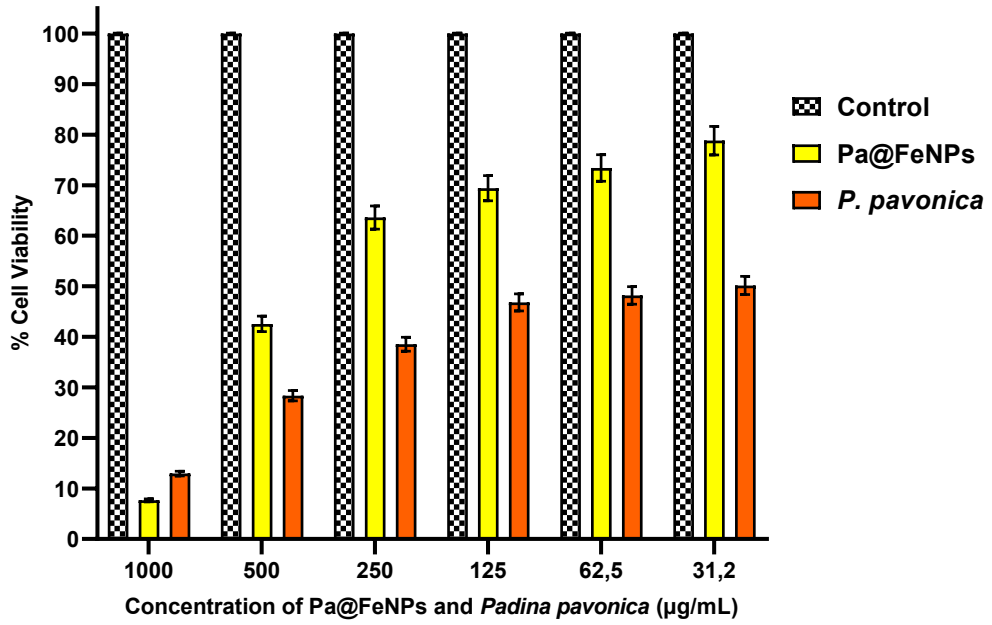

Figure 15. Effects of iron nanoparticles (Pa@FeNPs) on cell viability of Human neuroblastoma cell (SH-SY5Y) Statistical differences were observed at all treated concentrations compared to control ****p < 0.0001.

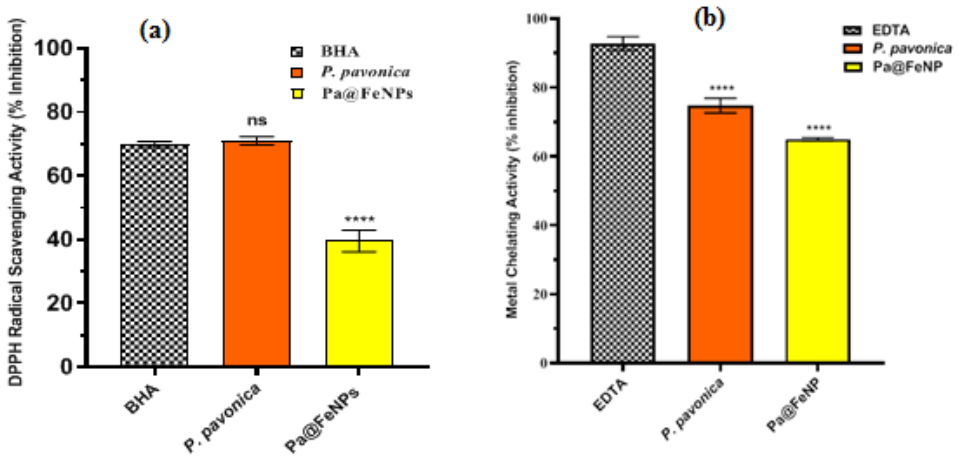

Figure 16. DPPH removal efficiency of *P. pavonica* and Pa@FeNPs (a), Metal-Chelating activity of *P. pavonica* and Pa@FeNP (b). Statistical analysis was performed with one-way ANOVA using Dunnett's multiple comparison test as a post-test with a confidence interval of ****p < 0.0001.

preparation. (Vitta et al., 2020; Ibrahim et al., 2019). The scavenging of the DPPH radical by Pa@FeNP may be related to the total flavonoids and polyphenol content in the extract, as well as the iron content of the nanoparticle. The content of polyphenolic compounds, including flavonoids, is closely related to antioxidant activity. The antioxidant content of polyphenolic compounds of *P. pavonica* has been determined in the literature (Caf et al., 2015; Ismail et al., 2019).

The Pa@FeNP nanoparticle showed significant metal chelating activity. The aqueous extract of *P. pavonica* and Pa@FeNP showed 74,71% and 64,95% metal-chelating activity, respectively (Figure 16a). Aqueous *P. pavonica* and Pa@FeNP extract showed significantly potent activity in the reference to EDTA, a synthetic antioxidant. Metal chelating magnetic iron oxide nanoparticles have wide applications in biological sciences and engineering (Yang & Su, 2011). In this sense, the metal chelating feature of this nanoparticle produced by green synthesis is a more reliable and environmentally friendly product for use.

Conclusion

Pa@FeNPs nanoparticle was successfully synthesized with a simple and green approach using the aqueous extract of *P. pavonica*. The study showed that nanoparticles prepared with *P. pavonica* are suitable adsorbent materials for adsorptive removal of CR dye from polluted wastewater with more than 95% dye removal rate. The particle level formed with polydisperse shapes was compatible with the Langmuir isotherm. Also, the monolayer structure showed that it is reusable and that the compounds on the surface do not interact with each other. The adsorption capacity observed with the highest percent removal level at 40 ^{o}C was also observed at 25^{o}C. Evaluating the photocatalytics is important in terms of its applicability since it was used in closed glass bottles without using any extra light source, only daylight in a laboratory environment. It is assumed that applying these two scenarios will provide high adsorption without any modification in a normal ecosystem. While the aqueous extract of *P. pavonica* showed neurotoxic effect at all concentrations studied, the neurotoxic effect IC_{50} value of Pa@FeNPs was determined as 400 µg/mL. Since this nanoparticle will be used in very low doses for CR removal in wastewater treatment systems, it is important that the neurotoxic IC_{50} value is set to 400 µg/mL which does not harm living things in the ecological chain. Also, Pa@FeNPs showed good iron chelating activity. The results indicate that Pa@FeNP may be used as dye removal and biological agent without harming environment.

Ethical Statement

Not applicable

Funding Information

This work is not supported by any funding

Author Contribution

Fatma CAF has done all the stages of this study

Conflict of Interest

The author(s) declare that they have no known competing financial or non-financial, professional, or personal conflicts that could have appeared to influence the work reported in this paper.

Acknowledgements

The author thanks Dr. Bülent KAYA, Semih GÖKDAĞ for providing all the facilities necessary for the completion of this study. I would like to thank Furkan DURUCAN for his contributions in the collection and identification of algae

References

Abboud Y., Saffaj T., Chagraoui A., El Bouari A., Brouzi K., Tanane O., & Ihssane, B. (2014). Biosynthesis, Characterization and Antimicrobial Activity of Copper Oxide Nanoparticles (Conps) Produced Using Brown Alga Extract (*Bifurcaria bifurcata*). *Applied Nanoscience,* 4(5), 571-576. https://doi.org/10.1007/s13204-013-0233-x

Abdul Salam, H., Rajiv, P., Kamaraj, M., Jagadeeswaran, P., Gunalan, S., & Sivaraj, R. (2012). Plants, Green Route for Nanoparticle Synthesis. *International Journal of Biological Sciences,* 1(5), 85-90.

Aksu, O., Yildirim, N.C., Danabas, D., & Yildirim, N. (2017). Biochemical Impacts of the Textile Dyes Remazol Brillant Blue and Congo Red On the Crayfish *Astacus leptodactylus* (Decapoda, Astacidae). *Crustaceana,* 90(13), 1563-1574. https://doi.org/10.1163/15685403-00003738

Ali, I. Al-Othman, Z.A., & Alwarthan A. (2016). Molecular Uptake of Congo Red Dye from Water on Iron Composite Nano Particles. *Journal of Molecular Liquids*, 224, 171. https://doi.org/10.1016/j.molliq.2016.09.108

Amini, S.M., & Akbari, A. (2019). Metal Nanoparticles Synthesis Through Natural Phenolic Acids. *IET Nanobiotechnology*, 13(8), 771-777. https://doi.org/10.1049/iet-nbt.2018.5386

Amini, S.M., Mohammadi, E., Askarian-Amiri, S., Azizi, Y., Shakeri-Zadeh, A., & Neshastehriz, A. (2021). Investigating The *in Vitro* Photothermal Effect of Green Synthesized Apigenin-Coated Gold Nanoparticle On Colorectal Carcinoma. *IET nanobiotechnology*, *15*(3), 329-337. https://doi.org/10.1049/nbt2.12016

Anjana, P.M., Bindhu, M.R., Umadevi, M., & Rakhi, R.B. (2018). Antimicrobial, Electrochemical and Photo Catalytic Activities of Zn Doped Fe_3O_4 Nanoparticles. *Journal of Materials Science: Materials in Electronics*, *29*(7), 6040-6050. https://doi.org/10.1007/s10854-018-8578-2

Ayadi, I., Mariza Monteiro, S., Regaya, I., Coimbra, A. Fernandes, F., Oliveira, M.M., Peixoto, F., & Mnif, W. (2015). Biochemical and Histological Changes in The

Liver and Gills Of Nile Tilapia *Oreochromis Niloticus* Exposed To Red 195 Dye. *RSC Advances*, 5, 87168-87178. https://doi.org/10.1039/C5RA13127H

Awad, N.E., Selim MA, Metawe, H.M., & Matloub A.A. (2008). Cytotoxic Xenicane Diterpenes from The Brown Alga *Padina pavonia* (L.) Gaill. *Phytotherapy Research,* 22, 1610-1613. https://doi.org/10.1002/ptr.2532

Azizi, S., Ahmad, M.B., Namvar, F., & Mohamad, R. (2014). Green Biosynthesis and Characterization of Zinc Oxide Nanoparticles Using Brown Marine Macroalga *Sargassum muticum* Aqueous Extract. *Materials letters,* 116, 275-277. https://doi.org/10.1016/j.matlet.2013.11.038

Azizi, S., Namvar, F., Mahdavi, M., Ahmad, M.B., & Mohamad, R. (2013). Biosynthesis of Silver Nanoparticles Using Brown Marine Macroalga, *Sargassum muticum* Aqueous Extract. Materials, 6, 5942-5950. https://doi.org/10.3390/ma6125942

Behura, R., Sakthivel, R., & Das, N. (2021). Synthesis of Cobalt Ferrite Nanoparticles from Waste Iron Ore Tailings and Spent Lithium Ion Batteries for Photo/Sono-Catalytic Degradation of Congo Red. *Powder technology*, 386, 519-527. https://doi.org/10.1016/j.powtec.2021.03.066

Bhattacharjee, S., Habib, F., Darwish, N., & Shanableh, A. (2021). Iron Sulfide Nanoparticles Prepared Using Date Seed Extract: Green Synthesis, Characterization and Potential Application for Removal of Ciprofloxacin and Chromium. *Powder technology*, 380, 219-228. https://doi.org/10.1016/j.powtec.2020.11.055

Bhoi, S.K. (2010). Adsorption characteristics of congo red dye onto PAC and GAC based on S/N ratio: A Taguchi Approach, Chemistry.

Caf, F., Yilmaz, Ö., Durucan, F., & Şen Özdemir N. (2015). Biochemical Components of Three Marine Macroalgae (*Padina pavonica, Ulva lactuca* and *Taonia atomaria*) from The Levantine Seacoast of Antalya, Turkey. *Journal of Biodiversity and Environmental Sciences*, 6, 401-411.

Cengiz, S., & Cavas, L. (2008). Removal of Methylene Blue by Invasive Marine Seaweed: *Caulerpa racemosa var.* Cylindracea. *Bioresource technology,* 99, 2357-2363. https://doi.org/10.1016/j.biortech.2007.05.011

Chandran, M., Yuvaraj, D., & Christudhas, L. (2016). Bio Synthesis of Iron Nanoparticles Using the Brown Seaweed, *Dictyota dicotoma*. *Indian Journal of Biotechnology*, 12(12), 112.

Chatterjee, S., Lee, M.W., & Woo, S.H. (2010). Adsorption of Congo Red by Chitosan Hydrogel Beads Impregnated with Carbon Nanotubes. *Bioresource Technology*, 101(6), 1800-1806. https://doi.org/10.1016/j.biortech.2009.10.051

Chatterjee, S., Chatterjee, S., Chatterjee, B.P., Das, A.R., & Guha, A.K. (2005). Adsorption of a Model Anionic Dye, Eosin Y, from Aqueous Solution by Chitosan Hydrobeads. *Journal of Colloid and Interface Science,* 288, 30-35. https:// doi.org/10.1016/j.jcis.2005.02.055

Chern, J.M., & Wu, C.Y. (2001). Desorption of Dye from Activated Carbon Beds: Effects of Temperature, pH, and Alcohol. *Water Research,* 35, 4159-4165. https://doi.org/10.1016/S0043-1354(01)00127-0

Cormaci, M., Furnari, G., Catra, M., Alongi, G., & Giaccone, G. (2012). Flora Marina Bentonica Del Mediterraneo: Phaeophyceae. *Bulletin of the Gioenian Academy of Natural Sciences,* 45, 1-508.

Deghrigue, M., Amri, S., Amor, H.B.H., Eltaief, N., Jacques, R., & Bouraoui, A. (2015). Phytochemical and Antiproliferative Activity of the Organic Extract and Its Semi-Purified Fractions from The Brown Alga *Padina pavonica*. *Journal of Pharmaceutical and Biological Sciences*, *3*(1), 2.

Dias, A.M., Hussain, A., Marcos, A.S., & Roque, A.A. (2011). Biotechnological Perspective On the Application of Iron Oxide Magnetic Colloids Modified with Polysaccharides. *Biotechnology Advances,* 29, 142-155. https://doi.org/10.1016/j.biotechadv.2010.10.003

Doğan, M., Karaoğlu, M.H., & Alkan, M. (2009). Adsorption Kinetics of Maxilon Yellow 4GL and Maxilon Red GRL Dyes On Kaolinite. *Journal of Hazardous Materials,* 165, 1142-1151. https://doi.org/10.1016/j.jhazmat.2008.10.101

Dubey, S.P., Dwivedi, A.D., Lahtinen, M., Lee, C., Kwon, Y.N., & Sillanpaa, M. (2013). Protocol for Development of Various Plants Leaves Extract in Single-Pot Synthesis of Metal Nanoparticles. *Spectrochimica Acta Part A: Molecular and Biomolecular Spectroscopy*, 103, 134-142.

El-Kassas, H.Y., Aly-Eldeen, M.A., & Gharib, S.M. (2016). Green Synthesis of Iron Oxide (Fe_3O_4) Nanoparticles Using Two Selected Brown Seaweeds: Characterization and Application for Lead Bioremediation. *Acta Oceanologica Sinica*, 35(8), 89-98. https://doi.org/10.1007/s13131-016-0880-3

Elmoubarki, R., Mahjoubi, F.Z., Tounsadi, H., Moustadraf, J., Abdennouri, M., Zouhri, A., El Albani, A., & Barka, N. (2015). Adsorption of Textile Dyes on Raw and Decanted Moroccan Clays: Kinetics, Equilibrium and Thermodynamics. *Water Resources and Industry*, 9, 16-29. https://doi.org/10.1016/j.wri.2014.11.001

Ercan, G., Uzunoğlu, D., Ergüt M., & Özer, A. (2019). Biosynthesis and Characterization of Iron Oxide Nanoparticles from *Enteromorpha Spp.* Extract: Determination of Adsorbent Properties for Copper (II) Ions. *International Journal of Current Advanced Research*, 3(1), 065-074.

Fawcett, D., Verduin, J., Shah, M., Sharma, B., & Poinern, D. (2017). A Review of Current Research into The Biogenic Synthesis of Metal and Metal Oxide Nanoparticles Via Marine Algae and Seagrasses. *Journal of Nanoscience*, 4, 1-15. https://doi.org/10.1155/2017/8013850

Flippo, E., Serra A., Buccolieri, A., & Manno, D. (2010). Green Synthesis of Silver Nanoparticles with Surose and Maltose: Morphological and Structural Characterization. *Journal of Non-Crystalline Solids,* 356, 344-350. https://doi.org/10.1016/j.jnoncrysol.2009.11.021

Francavilla, M., Pineda, A., Romero, A., Vargas, C., Monteleone, M., & Luque R. (2014). Efficient and Simple Reactive Milling Preparation of Photocatalytically Active Porous Zno Nanostructures Using Biomass Derived Polysaccharides*. Green Chemistry*, 16(5), 2876-2885. https://doi.org/10.1039/C3GC42554A

Freundlich, H. (1906). Concerning Adsorption in Solutions. *Zeitschrift Fur Physikalische Chemie-stochiometrie und Verwandtschaftslehre*, 57, 385-470. https://doi.org/10.1515/zpch-1907-5723.

Gautam, R.K., Mudhoo, A., & Chattopadhyaya, M.C. (2013). Kinetic, Equilibrium, Thermodynamic Studies and Spectroscopic Analysis of Alizarin Red S Removal by Mustard Husk. *Journal of Environmental Chemical Engineering,* 1, 1283-1291. https://doi.org/10.1016/j.jece.2013.09.021

Hatano, T., Kagawa, H., Yasuhara, T., & Okuda, T. (1988). Two New Flavonoids and Other Constituents in Licorice Root: Their Relative Astringency and Radical Scavenging Effects. *Chemical and Pharmaceutical Bulletin*, 36(6),

2090-2097. https://doi.org/10.1248/cpb.36.2090

Herrera-Becerra, R., Rius, J.L., & Zorrilla, C. (2010). Tannin Biosynthesis of Iron Oxide Nanoparticles. *Applied Physics A,* 100(2), 453-459.

Hou, H., Zhou, R., Wu, P., & Wu, L. (2012). Removal of Congo Red Dye from Aqueous Solution with Hydroxyapatite/Chitosan Composite. *Chemical Engineering Science*, 211-212, 336-342. https://doi.org/10.1016/j.cej.2012.09.100

Ibrahim, M., Shaltou, A.A., Atta, D.E., Jalbout, A.F., & Soylak, M. (2009). Removal of COOH, Cd and Pb Using Water Hyacinth: FTIR and Flame Atomic Absorption Study. *Journal of the Iranian Chemical Society,* 6(2), 364 372.https://doi.org/10.1007/BF03245846

Ibrahim, F.Y., EL-Khateeb, A.Y., & Mohamed, A.H. (2019). Rhus and Safflower Extracts as Potential Novel Food Antioxidant, Anticancer, and Antimicrobial Agents Using Nanotechnology. *Foods,* 8(4), 139. https://doi.org/10.3390/foods8040139

Iqbal, M.M., Imran, M., Hussain, T., Naeem, M.A., Al-Kahtani, A.A., Hah, G.M., Ahmad, S., Farooq, A., Rizwan, M., Majeed, A., Khan, A.R., & Ali S. (2021). Effective Sequestration of Congo Red Dye with Zno/Cotton Stalks Biochar Nanocomposite: Modeling, Reusability and Stability. *Journal of Saudi Chemical Society,* 25, 101176. https://doi.org/10.1016/j.jscs.2020.101176

Iram, M., Guo, C., Guan, Y., & Ishfaq, A. (2010). Adsorption and Magnetic Removal of Neutral Red Dye from Aqueous Solution Using Fe_3O_4 Hollow Nanospheres. *Journal of Hazardous Materials,* 181 (1), 1039-1050. https://doi.org/10.1016/j.jhazmat.2010.05.119

Ismail, G.A., Gheda, S.F., Abo-shady, A.M., & Abdel-karim, O.H. (2019). *In vitro* Potential Activity of Some Seaweeds as Antioxidants and Inhibitors of Diabetic Enzymes. *Food Science and Technology,* 40, 681-691. https://doi.org/10.1590/fst.15619.

Kataria, N., & Garg, V.K. (2017). Removal of Congo Red and Brilliant Green Dyes from Aqueous Solution Using Flower Shaped Zno Nanoparticles. *Journal of Environmental Chemical Engineering,* 5(6), 5420-5428. https://doi.org/10.1016/j.jece.2017.10.035

Khanehzaei, H., Ahmad, M.B., Shameli, K., & Ajdari, Z. (2014). Synthesis and Characterization of Cu@Cu_2O Core Shell Nanoparticles Prepared in Seaweed *Kappaphycus alvarezii* media. *International Journal of Electrochemical Science*, 9(12), 8189-8198.

Kopaç, T., & Sulu, E. (2019). Comparison of The Adsorption Behavior of Basic Red 46 Textile Dye on Various Activated Carbons Obtained from Zonguldak Coal. *Journal of the Faculty of Engineering and Architecture of Gazi University*, 34(3), 1227-1240

Kousha, M., Daneshvar, E., Dopeikar, H., Taghavi, D., & Bhatnagar, A. (2012). Box-Behnen Design Optimization of Acid Black 1 Dye Biosorption by Different Brown Macroalgae. *Chemical Engineering Journal*, 179,158-168. https://doi.org/10.1016/j.cej.2011.10.073

Ktari, L., & Guyot, M. (1999). A Cytotoxic Oxysterol from The Marine Alga *Padina pavonica* (L.) Thivy. *Journal of Applied Psychology,* 11, 511-513. https://doi.org/10.1023/a:1008162624027

Kumar, K., Dastidar, M.G., & Sreekrishnan, T.R. (2009). Effect of Process Parameters on Aerobic Decolourization of Reactive Azo Dye Using Mixed Culture. International *Journal of Biological, Biomolecular, Agri-cultural, Food and Biotechnological Engineering,* 3(10), 525-528.

Labena, A., Abdelhamid, A.E., Amin, A.S., Husien, S., Hamid, L., Safwat, G., Diab, A., Gobouri, A.A., & Azab, E. (2021). Removal of Methylene Blue and Congo Red Using Adsorptive Membrane Impregnated with Dried *Ulva fasciata* and *Sargassum dentifolium*. *Plants,* 10(2), 384. https://doi.org/10.3390/plants10020384

Langmuir, I. (1918). The Adsorption of Gases on Plane Surfaces of Glass, Mica and Platinum. *Journal of the American Chemical Society,* 40, 1361-1403. https://doi.org/10.1021/ja02242a004

Li, R., Liang, N., Ma, X., Chen, B., & Huang, F. (2019). Study on The Adsorption Behavior of Glycerin from Fatty Acid Methyl Esters by A Tertiary Amine-Type Anion Exchange Resin. *Journal of Chromatography A,* 1586, 62-71. https://doi.org/10.1016/j.chroma.2018.11.079

Ling, Y., Wei, K., Luo, Y., Gao, X., & Zhong, S. (2011). Dual Docetaxel/ Superparamagnetic Iron Oxide Loaded Nanoparticles for Both Targeting Magnetic Resonance Imaging and Cancer Therapy. *Biomaterials,* 32, 7139-7150. https://doi.org/10.1016/j.biomaterials.2011.05.089

Liu, J., Wang, N., Zhang, H., & Baeyens, J. (2019). Adsorption of Congo Red Dye On $Fexco_3$-Xo_4 Nanoparticles. *Journal of Environmental Management*, 238, 473-483. https://doi.org/10.1016/j.jenvman.2019.03.009

Luo, F., Yanga, D., Chena, Z., Megharaj, M., & Naidua, R. (2015). The Mechanism for Degrading Orange II Based On Adsorption and Reduction by Ion-Based Nanoparticles Synthesized by Grape Leaf Extract. *Journal of Hazardaous Materials,* 296, 37-45. https://doi.org/10.1016/j.jhazmat.2015.04.027

Mahdavi, M., Namvar, F., Ahmad, M.B., &, Mohamad, R. (2013). Green biosynthesis and characterization of magnetic iron oxide (Fe_3O_4) nanoparticles using seaweed (*Sargassum muticum*) aqueous extract. *Molecules,* 18(5), 5954-5964. https://doi.org/10.3390/molecules18055954

Mingyan, C., Yihong B., Jie, L., Yucheng, L., Ziying, W., & Xinkai, F. (2021). Adsorption Properties of Magnetic Sodium Ferrosilicate/Carboxymethyl Chitosan Composite with More Functional Groups and Surface Negative Potential. *Sustainable Chemistry and Pharmacy*, 24, 100519. https://doi.org/10.1016/j.scp.2021.100519.

Mohammadi, E., Amini, S.M., Mostafavi, S.H., & Amini, S.M. (2021). An Overview of Antimicrobial Efficacy of Curcumin-Silver Nanoparticles. *Nanomedicine Research Journal*, *6*(2), 105-111. https://doi.org/10.22034/NMRJ.2021.02.002

Mukherjee, A., Sarkar, D., & Sasmal, S. (2021). A Review of Green Synthesis of Metal Nanoparticles Using Algae. *Frontiers in Microbiology,* 12, 693899. https://doi.org/10.3389/fmicb.2021.693899

Nalci, O.B., Nadaroglu, H., Genc, S., Hacimuftuoglu, A., & Alayli, A. (2020). The Effects of Mgs Nanoparticles-Cisplatin-Bio-Conjugate on SH-SY5Y Neuroblastoma Cell Line. *Molecular Biology Reports*, 47, 9715-9723. https://doi.org/10.1007/s11033-020-05987-2

Namvar, F., Rahman, H.S., Mohamad, R., Baharara, J., Mahdavi, M., Amini, E., Chartrand, M.S., & Yeap, S.K. (2014). Cytotoxic Effect of Magnetic Iron Oxide Nanoparticles Synthesized Via Seaweed Aqueous Extract. *International Journal of Nanomedicine,* 9(1), 2479-2488. https://doi.org/10.2147/IJN.S59661

Nautiyal, P., Subramanian, K.A., & Dastidar, M.G. (2016). Adsorptive Removal of Dye Using Biochar Derived from

Residual Algae After In-Situ Transesterification: Alternate Use of Waste of Biodiesel Industry. *Journal of Environmental Management*, 1(182), 187-197. https://doi.org/10.1016/j.jenvman.2016.07.063

Neshastehriz, A., Amini, S. M., Mohammadi, A., Mahdavi, S.R., Mahabadi, V.P., & Akbari, A. (2020). *In-vitro* Investigation of Green Synthesized Gold Nanoparticle's Role in Combined Photodynamic and Radiation Therapy of Cancerous Cells. *Advances in Natural Sciences: Nanoscience and Nanotechnology*, 11(4), 045006. https://doi.org/10.1088/2043-6254/abb8c7.

Okath, K. (2016). Synthesis and Characterization of Iron Nanoparticles Using Banana Peels Extracts and Their Applicatıon in Aptasensor. Masters of Science, PhD Thesis. University of Nairobi. Nairobi.

Oliveira, A.C., de Araújo, A.R., Quelemes, P.V., Nadvorny, D., Soares-Sobrinho, J.L., de Almeida Leite, J.R.S., & da Silva, D.A. (2019). Solvent-free Production of Phthalated Cashew Gum for Green Synthesis of Antimicrobial Silver Nanoparticles. *Carbohydrate Polymers*, 213, 176-183.

Omezzine, F., Haouala, R., El Ayeb, A., & Boughanmi, N. (2009). Allelopathic and Antifungal Potentialities of *Padina pavonica* (L.) extract. *Journal of Plant Breeding and Crop Science,* 1, 094-203.

ur Rahman, O., Mohapatra, S.C., & Ahmad, S. (2012). Fe_3O_4 Inverse Spinal Super Paramagnetic Nanoparticles. *Materials Chemistry and Physics*, *132*(1), 196-202.

Ponnuchamy, K., & Jacob, J.A. (2016). Metal Nanoparticles from Marine Seaweeds-A Review. *Nanotechnology Reviews,* 5, 589-600. https://doi.org/10.1515/ntrev-2016-0010

Pugazhendhi, A., Prabhu, R., Muruganantham K., Shanmuganathan, R., & Natarajan, S. (2019). Anticancer, Antimicrobial and Photocatalytic Activities of Green Synthesized Magnesium, Oxide Nanoparticles (Mgonps) Using Aqueous Extract of *Sargassum wightii*. *Journal of Photochemistry and Photobiology B: Biology*, 190, 86-97. https://doi.org/10.1016/j.jphotobiol.2018.11.014

Prasad, C., Yuvaraja, G., & Venkateswarlu, P. (2017). Biogenic Synthesis of Fe_3O_4 Magnetic Nanoparticles Using *Pisum sativum* Peels Extract and Its Effect on Magnetic and Methyl Orange dye Degradation Studies. *Journal of Magnetism and Magnetic Materials*, 424, 376-381. https://doi.org/10.1016/j.jmmm.2016.10.084

Qasim, S., Zafar, A., Saif, M.S., Ali, Z., Nazar, M., Waqas, M., & Hasan, M. (2020). Green Synthesis of İron Oxide Nanorods Using *Withania coagulans* Extract İmproved Photocatalytic Degradation and Antimicrobial Activity. *Journal of Photochemistry and Photobiology B: Biology*, *204*, 111784. https://doi: 10.1016/j.jphotobiol.2020.111784.

Radu, M., Munteanu, M.C., Petrache, S., Serban, A.I., Dinu, D., Hermenean, A., Sima, C., & Dinischiotu, A. (2010). Depletion of intracellular glutathione and increased lipid peroxidation mediate cytotoxicity of hematite nanoparticles in MRC-5 cells. *Acta Biochimica Polonica*, 57(3), 355.https://doi.org/10.18388/abp.2010_2416

Rezaeian, A., Amini, S.M., Najafabadi, M.R.H., Farsangi, Z.J., & Samadian, H. (2021). Plasmonic hyperthermia or radiofrequency electric field hyperthermia of cancerous cells through green-synthesized curcumin-coated gold nanoparticles. *Lasers in Medical Science*, 1-9. https://doi.org/10.1007/s10103-021-03399-7

Rivas, F.J., Beltrán, F.J., Frades, J., & Buxeda, P. (2001). Oxidation of p-hydroxybenzoic Acid by Fenton's Reagent. *Water Research,* 35, 387-396. https://doi.org/10.1016/s0043-1354(00)00285-2

Sahayaraj, K., Sathiyamoorthy, R., & Rathi, J. (2012). Silver Nanoparticles Biosynthesis Using Marine Algae *Padina pavonica* (Linn.) and Its Microbial Activity. *Digest Journal Nanomater Biostruct* 7, 1557-1567.

Salem, D.M., Ismail M.M., & Tadros, H.R., 2020. Evaluation of the antibiofilm activity of three seaweed species and their biosynthesized iron oxide nanoparticles (Fe_3O_4-NPs). Egypt. *Egyptian Journal of Aquatic Research,* 46, 333-339. https://doi.org/10.1016/j.ejar.2020.09.001

Salem, D.M., Ismail, M.M., & Aly-Eldeen, M.A. (2019). Biogenic Synthesis and Antimicrobial Potency of Iron Oxide (Fe_3O_4) Nanoparticles Using Algae Harvested from The Mediterranean Sea. *Egypt. Egyptian Journal of Aquatic Research,* 45(3), 197-204. https://doi.org/10.1016/j.ejar.2019.07.002

Sathiyavimal, S., Vasantharaj, S., Bharathi, D., Saravanan, M., Manikandan, E., Kumar., S.S., & Pugazhendhi, A. (2018). Biogenesis of Copper Oxide Nanoparticles (Cuonps) Using *Sida acuta* and Their Incorporation Over Cotton Fabrics to Prevent the Pathogenicity of Gram Negative and Gram Positive Bacteria. *Journal of Photochemistry and Photobiology B: Biology*, 188, 126-134. https://doi.org/10.1016/j.jphotobiol.2018.09.014

Seki, H., Suzuki, A., & Mitsueda, S.I. (1998). Adsorption of Heavy Metal Ions on *Rhodobacter sphaeroides* and *Alcaligenes eutrophus* H16. *Journal of Colloid and Interface Science,* 197, 185-190. https://doi.org/10.1006/jcis.1997.5284

Shahwan, T., Abu Sirriah, S., Nairat, M., Boyacı, E., Eroğlu, A.E., Scott, T.B., & Hallam, K.R. (2011). Green Synthesis of Iron Nanoparticles and Their Application as A Fenton-Like Catalyst for The Degradation of Aqueous Cationic and Anionic Dyes. *Chemical Engineering Journal,* 172 (1), 258-266. https://doi.org/10.1016/j.cej.2011.05.103

Shakoor, S., & Nasar, A. (2016). Removal of Methylene Blue Dye from Artificially Contaminated Water Using Citrus Limetta Peel Waste as A Very Low Cost Adsorbent. *Journal of the Taiwan Institute of Chemical Engineers,* 66, 154-163. https://doi.org/10.1016/j.jtice.2016.06.009

Sharma, A., Sharma, S., Sharma, K., Chetri, S.P.K., Vashishtha A., Singh, P., Kumar, R., Rathi, B., & Agrawal, V. (2016). Algae as Crucial Organisms in Advancing Nanotechnology: A Systematic Review. *Journal of Applied Phycology,* 28(3), 1759-1774. https:// doi.org/10.1007/s10811-015-0715-1

Simonescu, C.M., Tătăruş, A., Culiţă, D.C., Stănică, N., Ionescu, I.A., Butoi, B., & Banici, A.M. (2021). Comparative Study of $CoFe_2O_4$ Nanoparticles and $CoFe_2O_4$-chitosan Composite for Congo Red and Methyl Orange Removal by Adsorption. *Nanomaterials,* 11(3), 711. https://doi.org/10.3390/nano11030711

Singh, K., Chopra, D.S., Singh, D., & Singh, N. (2020). Optimization and Ecofriendly Synthesis of Iron Oxide Nanoparticles as Potential Antioxidant. *Arabian Journal of Chemistry,* 13(12), 9034-9046. https:// doi.org/10.1016/j.arabjc.2020.10.025

Srilakshmi, C., &, Saraf, R. (2016). Ag-Doped Hydroxyapatite as Efficient Adsorbent for Removal of Congo Red Dye from Aqueous Solution: Synthesis, Kinetic and Equilibrium Adsorption Isotherm Analysis. *Microporous and Mesoporous Materials*, 219, 134-144. https://doi.org/10.1016/j.micromeso.2015.08.003

Subhashini, G., Ruban, P., &, Daniel, T. (2018). Biosynthesis and Characterization of Magnetic (Fe_3O_4) Iron Oxide Nanoparticles from A Red Seaweed *Gracilaria edulis* and

Its Antimicrobial Activity. *International Journal of Advanced Scientific Research and Management,* 3(10), 184-189.

Tatar, Ş., Serdar O., & Cıkcıkoğlu Yıldırım, N. (2019). Changes in Antioxidant and Detoxification Systems of the Freshwater Amphipod *Gammarus pulex* Exposed to Congo Red. *Journal of Animal Environmental Science,* 2, 76-81. https://doi.org/10.35229/jaes.542705

Temkin, M., & Pyzhev, V. (1940). Kinetics of Ammonia Synthesis on Promoted Iron Catalysts. *Acta Physicochimica U.R.S.S,* 12, 327-356.

Varadavenkatesan, T., Selvaraj, R., & Vinayagam, R. (2019). Dye Degradation and Antibacterial Activity of Green Synthesized Silver Nanoparticles Using *Ipomoea digitata* Linn. Flower Extract. *International Journal of Environmental Science and Technology*,16 (5), 2395-2404. https://doi.org/10.1007/s13762-018-1850-4

Vimonses, V., Lei, S., Jin, B., Chow, C.W.K., & Saint, C. (2009). Adsorption of Congo Red by Three Australian Kaolins. *Applied Clay Science,* 43(3-4), 465-472.https:// doi.org/10.1016/j.clay.2008.11.008

Wang, L., Li, J., Wang, Y., Zhao, L., & Jiang, Q. (2012). Adsorption Capability for Congo Red on Nanocrystalline Mfe2o4 (M =Mn, Fe Co, Ni) Spinel Ferrites. *Chemical Engineering Journal,* 181, 72-79. https://doi.org/10.1016/j.cej.2011.10.088

Wenli, Y., Yaping, Z., & Bo, S. (2004). The Radical Scavenging Activities of Radix Puerariae Isoflavonoids: A Chemiluminescence Study. *Food Chemistry,* 86(4), 525-529. https://doi.org/10.1016/j.foodchem.2003.09.005.

Vitta, Y., Figueroa, M., Calderon, M., & Ciangherotti, C. (2020). Synthesis of Iron Nanoparticles from Aqueous Extract of *Eucalyptus robusta* Sm and Evaluation of Antioxidant and Antimicrobial Activity. *Materials Science and Technology*, 3, 97-103. https://doi.org/10.1016/j.mset.2019.10.014

Xiaofan, L.V., Yiyang, M.A., Yangyang, L.İ., &Yang, Q.İ. (2020). Heterogeneous Fenton-Like Catalytic Degradation of 2,4-Dichlorophenoxyacetic Acid by Nano-Scale Zero-Valent Iron Assembled on Magnetite Nanoparticles. *Water,* 12(10), 2909. https://doi.org/10.3390/W12102909.

Xu, L., & Wang, J. (2011). A Heterogeneous Fenton-Like System with Nanoparticulate Zerovalent Iron for Removal of 4-chloro-3-methyl phenol. *Journal of Hazardous Materials,* 186, 256-264. https://doi.org/10.1016/j.jhazmat.2010.10.116.

Yagub, M.T., Sen, T.K., Afroze, S., & Ang H.M. (2014). Dye and Its Removal from Aqueous Solution by Adsorption A Review. *Advances in Colloid and Interface Science*, 209, 172-184. https://doi.org/10.1016/j.cis.2014.04.002.

Yang, K., & Su, W.W. (2011). Facile Synthesis of Metal-Chelating Magnetic Nanoparticles by Exploiting Organophosphorus Coupling. *Analytical Biochemistry*, 408(1), 175-177. https://doi.org/10.1016/j.ab.2010.09.014.

Yew, Y.P., Shameli, K., Miyake, M., Kuwano, N., Bt Ahmad Khairudin, N.B., Mohamad, S.E., & Lee, K.X. (2016). Green Synthesis of Magnetite (Fe_3O_4) Nanoparticles Using Seaweed (*Kappaphycus alvarezii*) Extract. *Nanoscale Research Letters*, 11(1), 276. https://doi.org/10.1186/s11671-016-1498-2.

Yoonus, J., Resmi, R., & Beena, B. (2021). Evaluation of Antibacterial and Anticancer Activity of Green Synthesized Iron Oxide (α-Fe_2O_3) nanoparticles. *Materials Today Proceedings*, 46, 2969-2974. https://doi.org/10.1016/j.matpr.2020.12.426.